Journal of Nuclear Medicine, published on August 12, 2019 as doi:10.2967/jnumed.119.226993

Molecular imaging of fibroblast activity after myocardial infarction using a ^{68}Ga-labelled fibroblast activation protein inhibitor FAPI-04

Running title: Imaging of fibroblast activity post-MI

Zohreh Varasteh[1], Sarajo Mohanta[2,3], Stephanie Robu[1], Miriam Braeuer[1], Yuanfang Li[2], Negar Omidvari[1], Geoffrey Topping[1], Ting Sun[2], Stephan G. Nekolla[1], Antonia Richter[1], Christian Weber[2,3], Andreas Habenicht[2], Uwe A. Haberkorn[4], Wolfgang A. Weber[1]

[1] Department of Nuclear Medicine, Klinikum rechts der Isar der TUM, Munich, Germany

[2] Institute for Cardiovascular Prevention, Ludwig-Maximilians-Universität (LMU), Munich, Germany

[3] German Centre for Cardiovascular Research (DZHK), partner site Munich Heart Alliance, Munich, Germany

[4] Department of Nuclear Medicine, University of Heidelberg, Heidelberg, Germany

Corresponding and first Author:

Zohreh Varasteh, PhD.

Department of Nuclear Medicine, Klinikum rechts der Isar der TUM

Ismaningerstrasse 22, 81675 Munich, Germany

Email: zohreh.varasteh@tum.de

Tel.: (+49) 89 4140 4558

Fax: (+49) 89 4140 4897

Word count: 5181

ABSTRACT

Heart failure (HF) remains a major source of late morbidity and mortality after myocardial infarction (MI). Temporospatial presence of the activated fibroblasts in the injured myocardium predicts the quality of cardiac remodelling post-MI. Therefore, monitoring of activated fibroblasts is of great interest for studying cardiac remodelling after MI. Fibroblast activation protein (FAP) expression is upregulated in activated fibroblasts. This study investigates the feasibility of imaging activated fibroblasts with a new ^{68}Ga-labelled FAP inhibitor (^{68}Ga-FAPI-04) for PET imaging of fibroblast activation in a preclinical model of MI. **Methods:** MI and sham-operated rats were scanned with ^{68}Ga-FAPI-04−PET/CT (1, 3, 6, 14, 23, and 30 days post-MI) and with ^{18}F-FDG (3 days post-MI). Dynamic ^{68}Ga-FAPI-04−PET and blocking studies were performed on MI rats, 7 days after coronary ligation. After in vivo scans, animals were euthanized and hearts were harvested for ex vivo analyses. Cryosections were prepared for autoradiography, haematoxylin and eosin (H&E), and immunofluorescence staining. **Results:** ^{68}Ga-FAPI-04 uptake in the injured myocardium peaked on day 6 after coronary ligation. The tracer accumulated intensely in the MI territory, as identified by decreased ^{18}F-FDG uptake and confirmed by PET/MR and H&E staining. Autoradiography and H&E staining of cross-sections revealed that ^{68}Ga-FAPI-04 accumulates mainly at the border zone of the infarcted myocardium. In contrast, there was only minimal uptake in the infarct of the blocked rats, comparable to the uptake in the remote non-infarcted myocardium (PET image-derived infarct-to-remote uptake ratio: 6±2). Immunofluorescence staining confirmed the presence of FAP-positive (FAP$^+$) myofibroblasts in the injured myocardium. Morphometric analysis of the whole heart sections demonstrated 3- and 8-fold higher FAP$^+$ fibroblast density in the border zone compared to infarct centre and remote area, respectively. **Conclusion:** ^{68}Ga-FAPI-04 represents a promising radiotracer for in vivo imaging of post-MI fibroblast activation. Non-

invasive imaging of activated fibroblasts may have significant diagnostic and prognostic values, which could aid clinical management of patients after MI.

Key words: Myocardial infarction, Cardiac remodelling, Fibroblast activation protein, Molecular imaging, PET

INTRODUCTION

Cardiac remodelling is a key factor for the prognosis of patients who survive a myocardial infarction (MI) (*1*). Adverse cardiac remodelling can lead to heart failure (HF), which is a major cause of morbidity and mortality world-wide (*2*). Post-MI fibrotic response plays a critical role in left ventricular (LV) remodelling (*3*). Activated cardiac fibroblasts have been identified as central mediators of this reparative response (*4*).

Following MI, fibroblasts undergo dynamic phenotypic changes and differentiate into collagen-secreting proto-myofibroblasts. These activated fibroblasts can further differentiate into mature myofibroblasts. Post-MI, activated fibroblasts migrate into the injured myocardium and contribute to tissue replacement, thereby helping to preserve the structural integrity of the infarcted heart. They secrete increased amounts of cytokines, growth factors, and peri-cellular proteases to maintain the extra cellular matrix (ECM) and promote replacement fibrosis−formation of a scar that stabilizes the ventricular wall and maintains the macroanatomy of the heart. Although the initial replacement/reparative fibrosis is pivotal for the prevention of ventricular wall rupture after an ischemic insult, it also induces geometrical, biomechanical, and biochemical changes in areas remote to the infarction and elicits the reactive/interstitial fibrosis. Excessive fibrosis and persistence of active fibroblasts within the myocardium can lead to increased LV stiffness and hence decreased cardiac contraction. Furthermore, the presence of excessive ECM may decrease oxygen and nutrient availability to the myocardium, contributing to detrimental cardiac remodelling. Non-invasive imaging of activated fibroblasts could therefore provide unique opportunities to study cardiac remodelling over time and to monitor therapeutic interventions that aim to prevent a progressive decline of ventricular function (*5,6*).

Fibroblast activation protein (FAP) is a homodimeric membrane-bound serine protease that has intracellular and extracellular soluble truncated forms. FAP is specifically expressed by activated fibroblasts during wound healing (*7*). Elevated expression of FAP in myofibroblasts has been reported in rat hearts with permanent MI and in the hearts of patients with acute MI (*8*). Recently, radiolabelled FAP inhibitors (FAPIs) for non-invasive imaging of FAP expression have been developed and characterized by Haberkorn and colleagues (*9,10*). PET imaging with radiolabelled FAPIs have shown desirable biodistribution and high uptake by activated stromal fibroblasts in murine experimental tumours, as well as in patients with different malignancies (*9,10*). In the present study, our objective was to evaluate the feasibility of imaging activated fibroblasts post-MI using a Gallium-68-labelled FAPI (^{68}Ga-FAPI-04).

MATERIALS AND METHODS

Experimental MI in Rats

A total of 20 Wistar rats (male, 3 month-old, 340−365 g, Charles River) were subjected to MI by permanent ligation of the left anterior descending (LAD) coronary artery. Animals were anesthetized by intramuscular administration of 0.5 mg/kg medetomidin (Pfizer), 5 mg/kg midazolam (Roche), and 0.05 mg/kg fentanyl (Ratiopharm) and artificially ventilated using a rodent ventilator for thoracotomy and permanent ligation of left coronary artery with 7−0 polypropylene suture. Successful coronary occlusions were verified visually by identification of cyanosis/paling of the myocardium downstream of the suture. Sham-operated animals (n=4) underwent the same surgical procedure except the ligation. Experiments were approved by the local

animal care committee and were in accordance with the German Animal Welfare Act (Regierung von Oberbayern, Munich, Germany).

Radiolabelling

^{68}Ga-labelling of FAPI-04 was performed in a fully automated, GMP compliant procedure using a GallElut^{+} synthesis module (Scintomics). A ^{68}Ge/^{68}Ga generator (iTHEMBA LABS) was eluted with 1.0 mol/L aq. HCl and a 1.2 mL fraction containing the highest activity (~500−600 MBq) was transferred into a reactor vial containing 20 nmol of FAPI-04 in 900 µL 2.7 mol/L HEPES in order to adjust the pH of the reaction mixture to 3.5. While heating to 95°C for 5 min, air was slowly bubbled through the solution for agitation. For purification, the reaction mixture was passed through a C18 light SPE cartridge (Waters), which was preconditioned by purging with ethanol (5 mL) and water (10 mL). The cartridge was rinsed with 10 mL water and ^{68}Ga-FAPI-04 was eluted from the cartridge with 2 mL ethanol/water (1/1, v/v), followed by purging with 1 mL PBS buffer (pH 7.4) and 1 mL water. For in vivo studies, ethanol was evaporated to exhibit the appropriate pH and osmolality for injection. Quality control of ^{68}Ga-FAPI-04 was performed using Radio-RP-HPLC and Radio-TLC.

In vivo (PET/CT) Imaging

Scans were acquired on a small-animal Inveon PET/CT scanner (Siemens). Static PET/CT images were acquired 1 h post-injection (p.i.) with ^{68}Ga-FAPI-04 (20−25 MBq, 4 nmol, 1, 3, 6, 14, 23, and 30 days post-MI) and ^{18}F-FDG (8−10 MBq, 3 days post-MI) with an acquisition time of 20 min. Images were reconstructed using Siemens Inveon software, which employs a 3-dimensional ordered subsets expectation maximum (OSEM3D) algorithm with attenuation

correction. Dynamic PET scans were acquired with ^{68}Ga-FAPI-04 (7 days post-MI) for 90 min. Acquired data were then Fourier rebinned in 46 time frames (6×5s, 21×10s, 8×120s, 8×300s, 3×600s) and reconstructed using the same OSEM3D algorithm. For quantification of tracer uptake, circular 2D regions of interest (ROIs) were placed on axial PET/CT images of the hearts and signal intensities were recorded as percentage of injected dose per gram of tissue (%ID/g). ROIs were drawn corresponding to the infarcted region and non-infarcted remote myocardium in the inferior septum.

Ex vivo (PET/MR) Imaging

In order to validate the results obtained by in vivo PET/CT imaging and to confirm the origin of the in vivo signal, one heart was also scanned ex vivo. On day 7 post-MI, a rat was injected with 60 MBq of ^{68}Ga-FAPI-04 and sacrificed 1 h p.i. The heart was excised and scanned using a small animal PET insert (MADPET4) for a 7 T MRI scanner (Agilent/GE MR901 magnet with Bruker AVANCE III HD electronics) with an acquisition time of 20 min. Anatomical MR images were acquired with a 3D spoiled gradient recalled echo (FLASH) sequence. In order to keep the LV open, the heart was filled with alginate impression material (Zitzmann). The same animal was scanned in vivo on day 6 post-MI with ^{68}Ga-FAPI-04–PET/CT.

Competition Experiment

To assess the specificity of ^{68}Ga-FAPI-04 accumulation and to confirm that uptake of ^{68}Ga-FAPI-04 in the injured myocardium is due to a saturable binding to FAP, a group of MI rats (n=3), referred to as the blocked group, was co-injected with blocking dose (550 nmol) of non-labelled

FAPI-04 to block specific binding sites 7 days after coronary ligation. The rats underwent PET/CT imaging followed by autoradiography. The same animals were scanned one day earlier (day 6 post-MI) with ^{68}Ga-FAPI-04–PET/CT without injection of the blocking compound.

Autoradiography and Histology

On day 7 post-MI, rats (n=3 MI non-blocked, n=3 MI blocked and n=2 sham) were injected with ^{68}Ga-FAPI-04 and sacrificed 1 h p.i. Serial short-axis cryosections of 10 μm-thickness were prepared from isolated hearts. Consecutive sections were used for autoradiography and haematoxylin and eosin (H&E) staining. The ex vivo spatial distribution of radioactivity in the heart cross-sections was examined using autoradiography. H&E staining was used to determine the location and extent of areas of infarction.

Immunofluorescence Staining and Quantification of FAP-positive Area

Cryosections were prepared from fresh frozen MI hearts (7 days post-MI), liver, lung, skin, and healthy hearts. Tissue sections were stained with antibodies against FAP (R&D) as marker of activated fibroblasts, prolyl-4-hydroxylase β (P4H) (Origene) as marker of activated and collagen-synthesizing fibroblasts, α-smooth muscle actin (SMA) (Merck) as marker to identify differentiated mature myofibroblasts, and vimentin (Merck) as general fibroblast marker, as described earlier (*8*). Stained sections were imaged using SP8 confocal laser scanning microscope and DM6000 fluorescence microscope (Leica). For imaging the entire surface of heart specimens, single-plane automated tile scans were acquired using a DM6 B Thunder imager 3D tissue (Leica) with a field of view of 5.5×5.5 mm^2, processed with Thunder software (Leica), and mosaic merged with 20%

overlaps. For morphometry of FAP^+ area in MI hearts, 3−5 parallel sections adjacent to H&E stained images were selected. H&E images were used to define the infarct centre, border, and remote area. FAP^+ areas were quantified within the selected areas using Image J (NIH). Image processing included changes in brightness, contrast and tonal range, and was applied equally across the entire image.

The experimental timeline of the in vivo and ex vivo studies are illustrated in Figure 1.

Statistics

Data are expressed as mean ± standard deviation (SD). The Mann-Whitney U test to compare two variables and one way ANOVA was used to compare multiple variables. A p-value ≤ 0.05 was considered to be significant. Statistical analysis was performed using SPSS Statistics software (version 24.0.0, IBM Company).

RESULTS

FAPI-04 was labelled with ^{68}Ga, with an overall radiochemical yield of 89±0.8% and radiochemical purity of ≥95%. The specific activity was 25−30 GBq/μmol.

Rapid Biodistribution and Accumulation of ^{68}Ga-FAPI-04 in the Myocardial Infarction

Figure 2A shows a series of dynamic images (axial and coronal sections) from 5 to 90 min p.i. of ^{68}Ga-FAPI-04 in MI heart (7 days post-MI). The images demonstrate rapid clearance of ^{68}Ga-FAPI-04 from circulation via renal excretion (Supplemental Fig. 1). Corresponding time-activity curves (average of 3 scans) for infarct and non-infarct remote areas show that the tracer

cleared gradually from infarcts and more rapidly from non-target remote tissue (Fig. 2B), resulting in increasing infarct-to-non-infarct tissue ratios over time (Fig. 2C).

Specific Uptake of ^{68}Ga-FAPI-04 in the Infarcts

In vivo longitudinal PET/CT images (axial sections) of a representative rat subjected to coronary ligation are shown in Figure 3A. The study was performed to assess the temporal presence of the activated fibroblasts in the injured myocardium. The ^{68}Ga-FAPI-04 uptake in the infarcts peaked on day 6 post-MI (Fig. 3B). Intense ^{68}Ga-FAPI-04 uptake (1.0±0.2 %ID/g) was observed in the hypometabolic MI territories that were identified on the ^{18}F-FDG−PET/CT scans. Additionally, an ex vivo 7 T PET/MR scan of the heart of one rat was performed in order to better localize the ^{68}Ga-FAPI-04 signal within the intact myocardium (Fig. 4). Fusion of PET and high resolution MR confirmed that ^{68}Ga-FAPI-04 accumulated within the infarcted myocardial region. In vivo PET image-derived infarct-to-remote myocardium uptake ratio was 6±2, 6 days post-MI (Fig. 5B). Uptake ratios relative to other organs were also high and are summarized in Supplemental Table 1. Thus, the infarcted myocardium was imaged with high contrast 6 days after coronary ligation. The saturation of FAP by co-injection of non-labelled FAPI-04 decreased the ^{68}Ga-FAPI-04 signal dramatically in the infarct region (0.21±0.08 %ID/g, p=0.01), to the same level as in the sham-operated rats (0.23±0.06 %ID/g). Similarly, co-injection of non-labelled FAPI-04 also decreased uptake of ^{68}Ga-FAPI-04 within the surgical wound to the background level (Fig. 5A). The exact location of ^{68}Ga-FAPI-04 uptake within the myocardium was further analysed by autoradiography and correlated with histological findings. In autoradiography images, increased uptake of ^{68}Ga-FAPI-04 was predominantly observed in peri-infarct border zone (Fig. 6). No significant tracer uptake was observed in the remote uninvolved myocardial regions or in the myocardium of sham-operated rats (Fig. 5A). The infarct-to-remote myocardium signal intensity

ratio was 14.1±0.8 (Fig. 5C). Blocking of the binding sites with excess amount of non-labelled FAPI-04 decreased the infarct-to-non-infarct signal intensity ratio 10-fold to 1.4±0.2 (p=0.02).

FAP is Expressed by Activated Fibroblasts in the Peri-infarcted Myocardium

To determine FAP expression in the myocardial connective tissue, multi-colour immunofluorescence staining analyses were performed in infarcted rat hearts at 7 days post-MI. Thunder imaging of the entire heart slices revealed that FAP^+ cells were selectively accumulated in the peri-infarcted area rather than in the infarct centre or remote healthy myocardium (Fig. 7A). Within the infarcted hearts, few FAP^+ fibroblasts were located in the necrotic/fibrotic infarct area, but rarely detected in the remote myocardium (Fig 7A; Supplemental Fig. 2) or in the myocardium of healthy hearts (Supplemental Fig. 3). Enumeration of FAP^+ cells in the selected areas of MI hearts revealed 3- and 8-fold higher FAP^+ fibroblast density in the border zones compared to infarct centre and remote areas, respectively (Fig. 7B). In the peri-infarcted connective tissue, majority of FAP^+ cells strongly expressed P4H, while fewer FAP^+ cells expressed SMA (Fig. 7D) indicating massive infiltration of FAP^+ $P4H^+$ proto-myofibroblasts in the infarct border zone. These data were consistent with previously published data on FAP expression after MI (8). Co-expression analyses of vimentin with FAP in liver, lung and skin demonstrated FAP expression in dermal $vimentin^+$ fibroblasts only (Supplemental Fig. 3) confirming the presence of activated fibroblast in skin as evidenced by others (*11*).

DISCUSSION

The present study demonstrated the feasibility of imaging activated fibroblasts after MI using PET and the radiolabelled FAP inhibitor ^{68}Ga-FAPI-04. Fibroblast activity in the infarcted

myocardium was imaged with PET/CT, with high contrast and with minimal uptake in normal myocardium (infarct-to-remote myocardium uptake ratio was 6±2, 6 days post-MI) or other organs such as the liver (infarct-to-liver uptake ratio was 11±3, 6 days post-MI). The specificity of the PET signal was confirmed by blocking with non-labelled FAPI-04 and immunofluorescence staining studies corroborating high expression of FAP by activated fibroblasts. Furthermore, the study showed the feasibility of imaging the time course of fibroblast activation after MI. Peak activity was observed 6 days after coronary ligation which decreased rapidly to the background level, already two weeks after infarction. The signal from ^{68}Ga-FAPI-04 is therefore fundamentally different from contrast enhancement on MRI which persists for months in the myocardium after infarction. Thus, ^{68}Ga-FAPI-04 shows fibroblast activation and fibrosis formation whereas MRI visualizes the presence of fibrous tissue independent from the activation state of the fibroblasts.

Identification of drugs that selectively inhibit fibroblast activation and transdifferentiation to the ECM-secreting myofibroblast cell state represents an attractive approach for the treatment of fibrosis-related diseases which include not only myocardial infarction, but also other common diseases such as liver cirrhosis or pulmonary fibrosis (*12*). Anti-fibrotic treatments inhibiting the pathways responsible for interconversion of quiescent fibroblasts to activated and profibrotic myofibroblasts have shown promise for improving left ventricular function in preclinical studies (*13-15*). However, translation of experimental findings into human patients has been rather limited. One reason is the lack of tools to non-invasively monitor fibroblast activation in patients. Specifically, the favourable roles of myofibroblasts in early infarct healing and detrimental effects of prolonged increase of reactive fibrosis require cautious timing for safe and effective anti-fibrotic treatments. It is therefore conceivable that a diagnostic strategy targeted at detecting active myofibroblasts would allow for a better understanding of their temporospatial presence in the

injured myocardium, estimation of the likelihood of post-infarction HF evolution, and assessment of the efficacy of anti-fibrosis therapies.

Expansion of fibrosis in areas remote to the infarction, known as reactive fibrosis, is believed to be an important mechanism for the development of HF (*3*). In the present study we did not observe an increased uptake of ^{68}Ga-FAPI-04 in the remote uninjured myocardium. However, it is important to note that experiments were performed in healthy rats that did not show signs of HF during the relatively short follow-up period. Future studies in animals with risk factors for the development of post-MI HF, e.g. diabetes (*16*) or hyperlipidaemia (*17*), are required in order to assess the ability of ^{68}Ga-FAPI-04 to monitor fibrosis formation in the area remote to the injured myocardium.

Several candidate biological processes have been targeted for molecular imaging of cardiac fibrosis and variety of ECM components have been tested to this aim (*18*). However, fibrosis is the consequence or end-point of the fibroblast activation. Once fibrosis has developed it will generally be challenging to reverse the deposition of collagen and other proteins in the ECM. In contrast, evaluation of fibroblast activation provides indirect evidence of the rate of fibrogenesis or collagen deposition, and hence may identify a time window during which fibrosis can still be prevented and the disease course altered.

Upregulated expression of $\alpha_v\beta_3$ in activated fibroblasts has been reported in vitro and in vivo (*18,19*). In some proof of concept studies, an RGD imaging peptide (RIP) has been used to identify proliferating myofibroblasts in post-infarct animal models (*20,21*), and in patients (*22*). However, preclinical and clinical studies documented that $\alpha_v\beta_3$ integrin is expressed not only by activated cardiac myofibroblasts but also by macrophages (*23*) and within endothelial cells of the microvasculature (*24-26*). Therefore, even though $\alpha_v\beta_3$ expression may hold promise as a combined

marker of post-MI healing activity (fibroblast activation, inflammation, and angiogenesis), it is not exclusive to be specific for activated fibroblasts (*6*).

The expression of FAP in myocardial fibroblast subsets was first demonstrated by Tillmanns et al. in frozen sections from rat hearts subjected to permanent LAD ligation and in paraffin-embedded formalin-fixed tissue samples obtained from the LV apex of MI patients (*8*). It was clearly shown that FAP^+ cells were indeed activated fibroblasts, predominantly proto-myofibroblasts, as evidenced by co-expression of FAP with P4H, SMA, and vimentin in rat hearts, and with Thy-1 in human hearts (*8*). The researchers then concluded that FAP expression identifies collagen synthesizing activated, but not resting, fibroblasts. Therefore, imaging FAP expression provides unique opportunities to study fibroblast activity in the injured myocardium.

Based on a small molecule enzyme inhibitor with high affinity to FAP (*27*), series of novel FAPI conjugates (n=15, FAPI-01 to 15) were developed by several approaches of chemical modifications (*9,10*). Among other quinolone-based radiopharmaceuticals, FAPI-04 showed improved pharmacokinetic properties regarding target accumulation and retention time (*10*). The comprehensive preclinical evaluation of the tracer led to the clinical translation of FAPI-04 for the diagnosis and therapy of metastasized cancer patients (*10*). These initial patient studies showed high uptake of ^{68}Ga-FAPI-04 by several malignancies and only very low uptake by lung, liver, and kidneys. Therefore, we expect that imaging of fibroblast activation post-MI will also be feasible in humans using ^{68}Ga-FAPI-04.

We realize the following limitations of our initial evaluation of FAP imaging of myocardial fibroblasts. First, we imaged the regional presence of activated fibroblasts in the infarcts only after permanent coronary artery occlusion and observed that ^{68}Ga-FAPI-04 accumulated predominantly in the border region. This tracer uptake pattern in the infarct area may be partially attributed to

inadequate delivery of radiotracer to the infarct area due to no-reflow or poor collateral flow to the infarct central region. Future studies are required to assess ^{68}Ga-FAPI-04 uptake after myocardial infarct in ischemia/reperfusion models. These studies are required to assess if ^{68}Ga- FAPI-04 can image the effect of coronary interventions on the extent of fibroblast activation. However, permanent LAD ligation model used in our study is likewise clinically relevant in that it allows the study of fibroblast activation after MI in the absence of potential confounding effects of reperfusion (*28*). Additionally, the potential of ^{68}Ga-FAPI-04 for imaging diffuse fibrosis needs to be evaluated in proper animal models, e.g. a pressure-overload-induced disease model. These studies are required to determine how sensitively ^{68}Ga-FAPI-04 can detect myofibroblasts, i.e. what density of myofibroblasts is required for a quantifiable signal. However, the very strong in vivo signal obtained after MI (1.0±0.2 %ID/g, day 6 post-MI) in the present study, as well as the very low uptake in non-infarcted myocardium (0.2±0.1 %ID/g, day 6 post-MI) and neighbouring normal organs suggests that more subtle forms of fibroblast activation will also be detectable by ^{68}Ga-FAPI-04−PET/CT. Finally, due to the presence of high ^{68}Ga-FAPI-04 uptake in the surgical wound region in close proximity of the infarct area, it was not possible to quantify in vivo PET signal from the infarcts. To avoid the surgical trauma by thoracotomy in open-chest models of coronary ligation and to provide temporal information of FAP expression changes after MI in a non-invasive and quantitative mode, closed-chest catheter-based models of MI are proposed for future studies.

CONCLUSION

Activation of fibroblasts was imaged non-invasively with high contrast using PET and the FAP inhibitor ^{68}Ga-FAPI-04. We expect that the ability to study activated fibroblasts non-invasively and repetitively will provide new insights into ventricular remodelling post-MI and

possibly also other cardiac pathologic conditions that are associated with activation of fibroblasts, e.g. hypertension and ischemic, dilated, and hypertrophic cardiomyopathies (*15*). Further studies of the feasibility of imaging fibroblast activation with ^{68}Ga-FAPI-04−PET/CT in the various settings are warranted.

ACKNOWLEGMENTS

The authors thank Sybille Reder and Markus Mittelhäuser for their technical assistance in PET/CT scans.

DISCLOSURE

This research was financially supported by Deutsches Zentrum für Herz-Kreislaufforschung (DZHK). Andreas Habenicht and Sarajo Mohanta were supported by Deutsche Forschungsgemeinschaft (DFG): HA 1083/15-4 (AH) and MO 3054/1-1 (SM). The authors do not have any conflicts of interest to declare.

Key points

QUESTION: Is it feasible to dynamically monitor cardiac fibroblast activation after MI with ^{68}Ga-FAPI-04−PET?

PERTINENT FINDINGS: Temporospatial presence of activated fibroblasts in the infarcted myocardium was imaged using ^{68}Ga-FAPI-04−PET/CT. The local accumulation of ^{68}Ga-FAPI-04 was peaked on day 6 post-MI, mainly in the infarct border zone.

IMPLICATIONS FOR PATIENT CARE: Non-invasive detection of active fibroblasts would help the clinicians to assess the likelihood of evolution of HF after MI and to monitor the efficacy of anti-fibrosis therapies.

REFERENCES

1. Mendis S, Puska P, Norrving B. Global Atlas on Cardiovascular Disease Prevention and Control. World Health Organization, Geneva; 2011:3–18

2. Bahit MC, Kochar A, Granger CB. Post-myocardial infarction heart failure. *JACC Heart Fail*. 2018;6:179–186.

3. Talman V, Ruskoaho H. Cardiac fibrosis in myocardial infarction−from repair and remodelling to regeneration. *Cell Tissue Res*. 2016;365:563–581.

4. van den Borne SW, Diez J, Blankesteijn WM, Verjans J, Hofstra L, Narula J. Myocardial remodelling after infarction: the role of myofibroblasts. *Nat Rev Cardiol*. 2010;7:30–37.

5. Rog-Zielinska EA, Norris RA, Kohl P, Markwald R. The living scar-cardiac fibroblasts and the injured heart. *Trends Mol Med*. 2016;22:99–114.

6. de Haas HJ, van den Borne SW, Boersma HH, Slart RH, Fuster V, Narula J. Evolving role of molecular imaging for new understanding: targeting myofibroblasts to predict remodeling. *Ann N Y Acad Sci*. 2012;1254:33–41.

7. Garin-Chesa P, Old LJ, Rettig WJ. Cell surface glycoprotein of reactive stromal fibroblasts as a potential antibody target in human epithelial cancers. *Proc Natl Acad Sci USA*. 1990;87:7235−7239.

8. Tillmanns J, Hoffmann D, Habbaba Y, et al. Fibroblast activation protein alpha expression identifies activated fibroblasts after myocardial infarction. *J Mol Cell Cardiol*. 2015;87:194–203.

9. Loktev A, Lindner T, Mier W, et al. A tumor-imaging method targeting cancer-associated fibroblasts. *J Nucl Med.* 2018;59:1423–1429.

10. Lindner T, Loktev A, Altmann A, et al. Development of quinoline-based theranostic ligands for the targeting of fibroblast activation protein. *J Nucl Med*. 2018;59:1415–1422.

11. Janson DG, Saintigny G, van Adrichem A, Mahé C, El Ghalbzouri A. Different gene expression patterns in human papillary and reticular fibroblasts. *J Invest Dermatol*. 2012;132:2565–2572.

12. Bollong MJ, Yang B, Vergani N, et al. Small molecule-mediated inhibition of myofibroblast transdifferentiation for the treatment of fibrosis. *Proc Natl Acad Sci U S A*. 2017;114:4679-4684.

13. Thum T, Gross C, Fiedler J, et al. MicroRNA-21 contributes to myocardial disease by stimulating MAP kinase signalling in fibroblasts. *Nature*. 2008;456:980–984.

14. Bradley JM, Spaletra P, Li Z, et al. A novel fibroblast activation inhibitor attenuates left ventricular remodeling and preserves cardiac function in heart failure. *Am J Physiol Heart Circ Physiol.* 2018;315:H563−H570.

15. Creemers EE, Pinto YM. Molecular mechanisms that control interstitial fibrosis in the pressure-overloaded heart. *Cardiovasc Res*. 2011;89:265–272.

16. Greer JJ, Ware DP, Lefer DJ. Myocardial infarction and heart failure in the db/db diabetic mouse. *Am J Physiol Heart Circ Physiol*. 2006;290:H146–53.

17. Maczewski M, Maczewska J. Hypercholesterolemia exacerbates ventricular remodelling in the rat model of myocardial infarction. *J Card Fail*. 2006;12:399–405.

18. de Haas HJ, Arbustini E, Fuster V, Kramer CM, Narula J. Molecular imaging of the cardiac extracellular matrix. *Circ Res*. 2014;114:903–915.

19. Asano Y, Ihn H, Yamane K, Jinnin M, Mimura Y, Tamaki K. Increased expression of integrin alpha(v)beta3 contributes to the establishment of autocrine TGF-beta signaling in scleroderma fibroblasts. *J Immunol*. 2005;175:7708–7718.

20. van den Borne SW, Isobe S, Verjans JW, et al. Molecular imaging of interstitial alterations in remodeling myocardium after myocardial infarction. *J Am Coll Cardiol*. 2008;52:2017–2028.

21. van den Borne SW, Isobe S, Zandbergen HR, et al. Molecular imaging for efficacy of pharmacologic intervention in myocardial remodeling. *JACC Cardiovasc Imaging*. 2009;2:187–198.

22. Verjans J, Wolters S, Laufer W, et al. Early molecular imaging of interstitial changes in patients after myocardial infarction: comparison with delayed contrast-enhanced magnetic resonance imaging. *J Nucl Cardiol*. 2010;17:1065–1072.

23. Antonov AS, Kolodgie FD, Munn DH, Gerrity RG. Regulation of macrophage foam cell formation by alphaVbeta3 integrin: potential role in human atherosclerosis. *Am J Pathol*. 2004;165:247–258.

24. Meoli DF, Sadeghi MM, Krassilnikova S, et al. Noninvasive imaging of myocardial angiogenesis following experimental myocardial infarction. *J Clin Invest*. 2004;113:1684–1691.

25. Brooks P, Clark R, Cheresh D. Requirements of vascular integrin avb3 for angiogenesis. *Science.* 1994;264:569–571.

26. Jenkins WS, Vesey AT, Stirrat C, et al. Cardiac $\alpha v\beta_3$ integrin expression following acute myocardial infarction in humans. *Heart*. 2017;103:607–615.

27. Jansen K, Heirbaut L, Cheng JD, et al. Selective inhibitors of fibroblast activation protein (FAP) with a (4-Quinolinoyl)-glycyl-2-cyanopyrrolidine scaffold. *ACS Med Chem Lett*. 2013;4:491–496.

28. Hausenloy DJ, Yellon DM. Myocardial ischemia-reperfusion injury: a neglected therapeutic target. *J Clin Invest*. 2013;123:92–100.

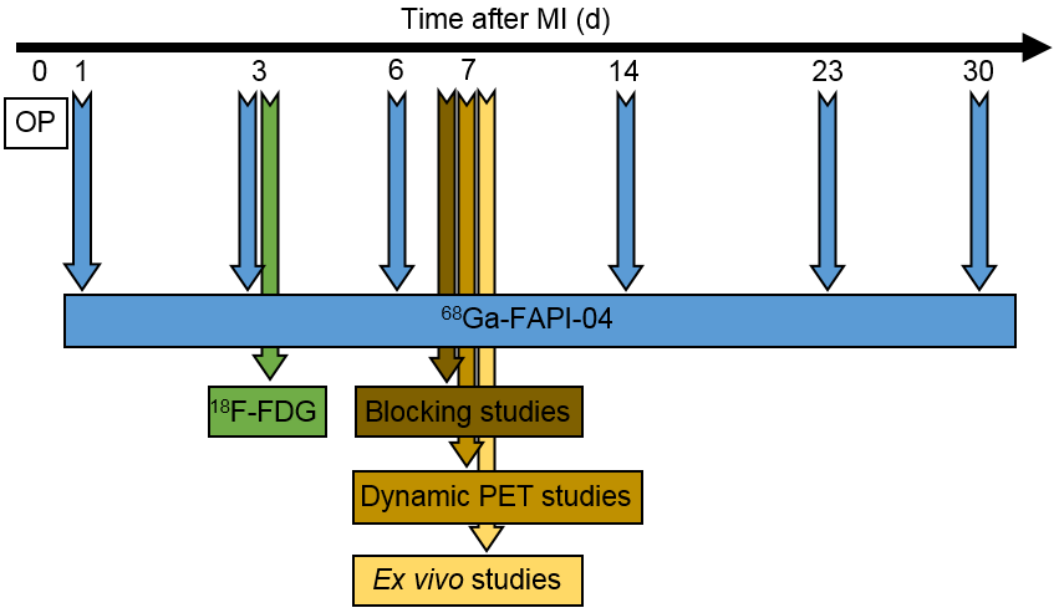

FIGURE. 1 Experimental timeline. OP stands for operation.

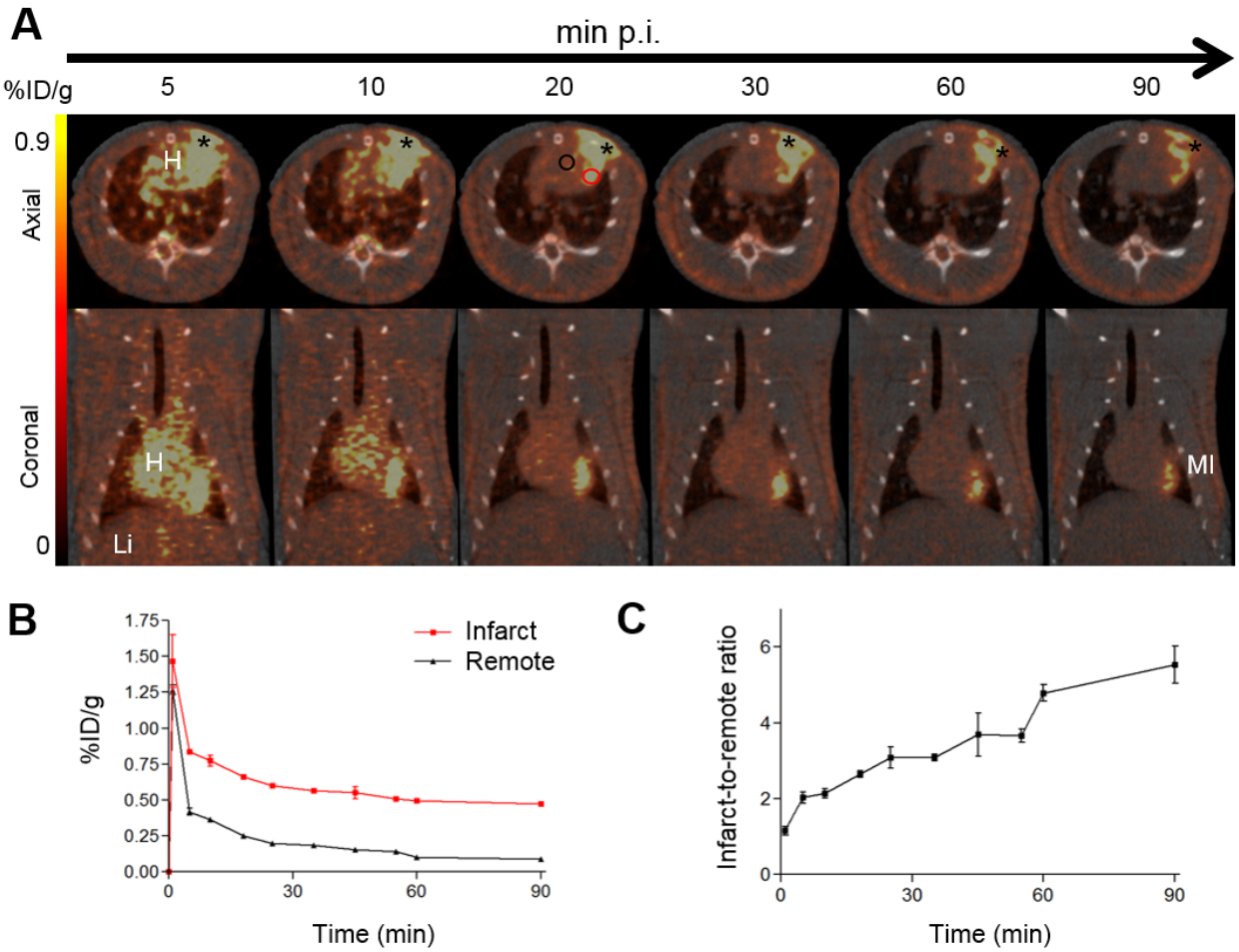

FIGURE. 2 In vivo dynamic imaging of ^{68}Ga-FAPI-04 uptake. (A) Serial PET/CT images (axial and coronal sections) from a 90-min dynamic scan of MI rat, 7 days after coronary ligation. The representative ROIs (2D) drawn over the infarct border zone and remote myocardium are illustrated in red and black circles, respectively. The ROIs in the infarcts were placed relatively far from the surgical wounds. Of note, ^{68}Ga-FAPI-04 exhibited elevated uptake in the scars from operation (asterisk). (B) Corresponding time–activity curves for infarcted and non-infarcted heart tissue (average and SD, n=3). (C) Infarct-to-non-infarct ratio over time (average and SD, n = 3). H stands for heart; Li, liver; MI, myocardial infarction.

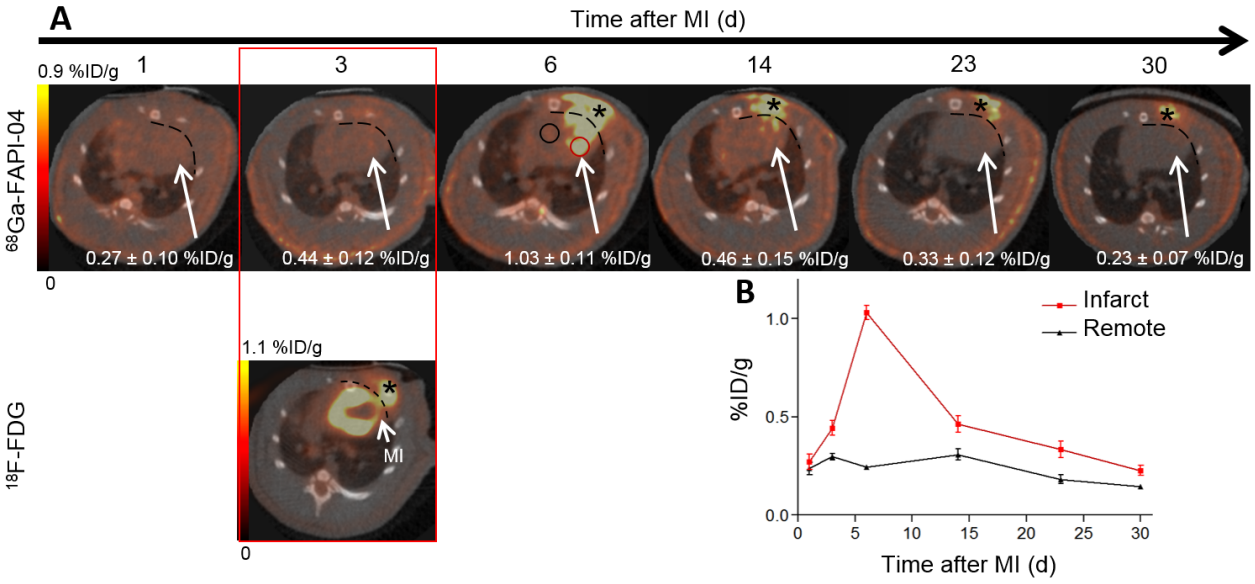

FIGURE. 3 In vivo imaging of ^{68}Ga-FAPI-04 uptake in a longitudinal study. (A) Static PET/CT matched axial slices in the same rat subjected to coronary ligation and scanned 1 h p.i. of ^{68}Ga-FAPI-04 (1, 3, 6, 14, 23, and 30 days post-MI) and ^{18}F-FDG (3 days post-MI). Dashed lines separate the tracer uptake in the myocardium from the uptake in the surgical wounds. In the 6 days post-MI image, the representative ROIs (2D) drawn over the infarct border zone and remote myocardium are illustrated in red and black circles, respectively. ^{68}Ga-FAPI-04 uptake in the ROIs of infarcts is demonstrated. (B) Corresponding time–activity curves for infarcted and non-infarcted heart tissue (average and SD, n=3). ^{68}Ga-FAPI-04 and ^{18}F-FDG exhibited elevated uptake in the scars from operation (asterisk).

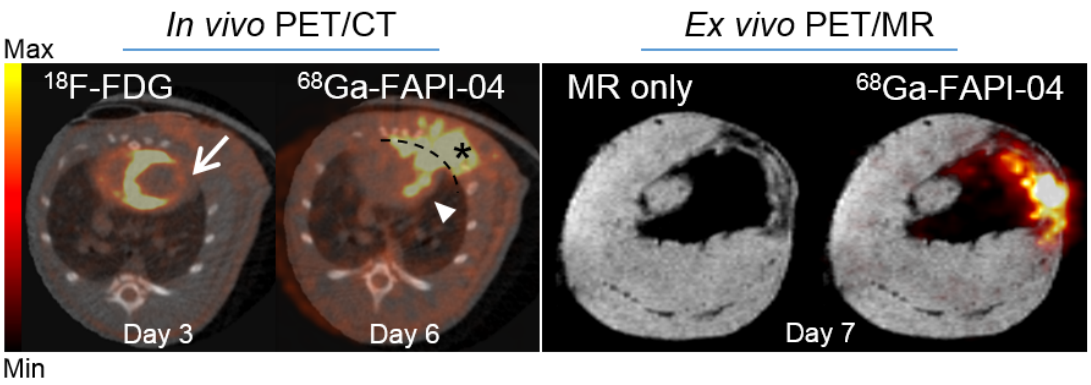

FIGURE. 4 Axial sections of in vivo PET/CT imaging with ^{18}F-FDG (day 3 post-MI) and ^{68}Ga-FAPI-04 (day 6 post-MI) and corresponding ex vivo PET/MR imaging with ^{68}Ga-FAPI-04 (day 7 post-MI). ^{18}F-FDG image was used to identify areas of infarcted myocardium (arrow), where increased uptake of ^{68}Ga-FAPI-04 was apparent (arrow head). ^{68}Ga-FAPI-04 exhibited an elevated uptake in the post-surgical scar (asterisk). Dashed line separates ^{68}Ga-FAPI-04 uptake in the myocardium from the surgical wound. The high resolution MR and PET/MR data confirmed the infarcted area, where ^{68}Ga-FAPI-04 uptake was increased.

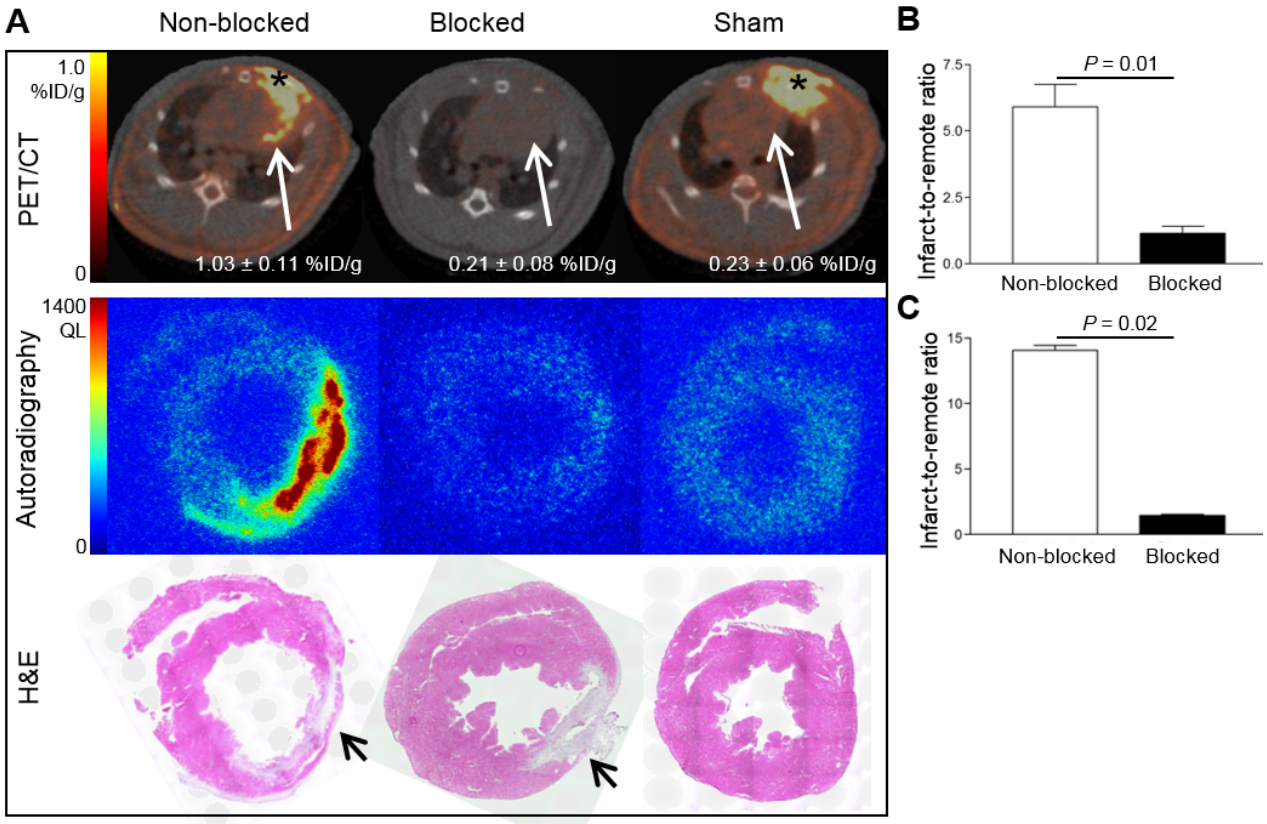

FIGURE. 5 Binding specificity test. (A) PET/CT axial views (upper panel), autoradiographs (middle panel) and corresponding H&E stainings (lower panel) of 10-µm cross-sections prepared from MI non-blocked, blocked, and sham-operated rats. Autoradiographs and corresponding H&E stainings from non-blocked rat hearts show an increased ^{68}Ga-FAPI-04 uptake in the infarcted area at 7 days after MI, whereas uptake is negligible after sham-operation or injection of non-labelled FAPI-04 (blocked). Infarcted areas in H&E stainings are identified with black arrows. (B) PET image-derived infarct-to-remote myocardium uptake ratio (derived from n=6 non-blocked and n=3 blocked rat hearts subjected to coronary ligation). (C) Autoradiography image-derived infarct-to-remote myocardium uptake ratio (derived from n=3 non-blocked and n=3 blocked MI hearts).

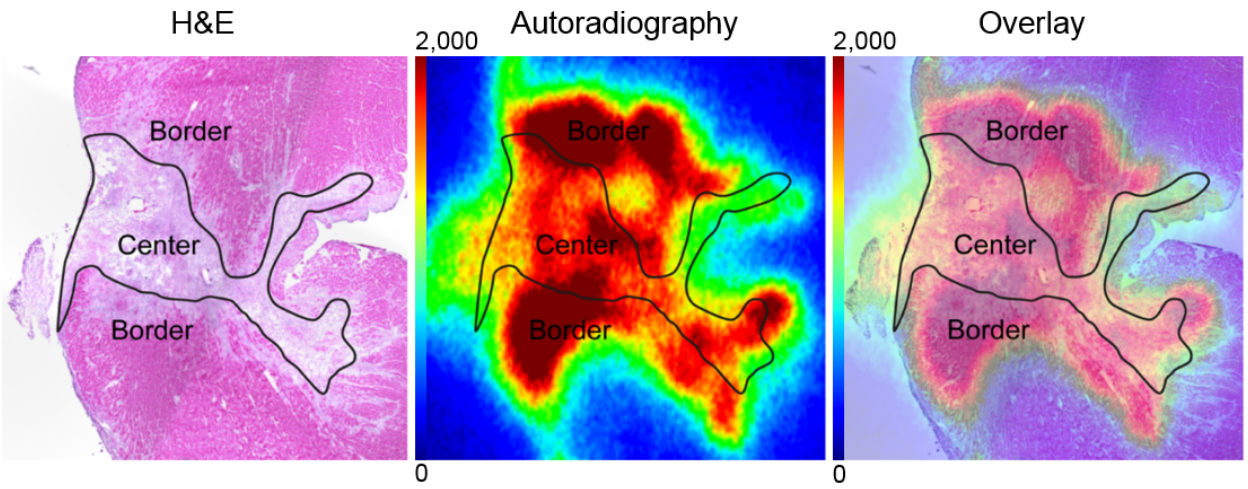

FIGURE. 6 Ex vivo evaluation of ^{68}Ga-FAPI-04 uptake in the infarct at 7 days post-MI. Representative autoradiograph and corresponding H&E staining from a rat heart show elevated and heterogeneous uptake of ^{68}Ga-FAPI-04 in the infarct border compared to infarct centre.

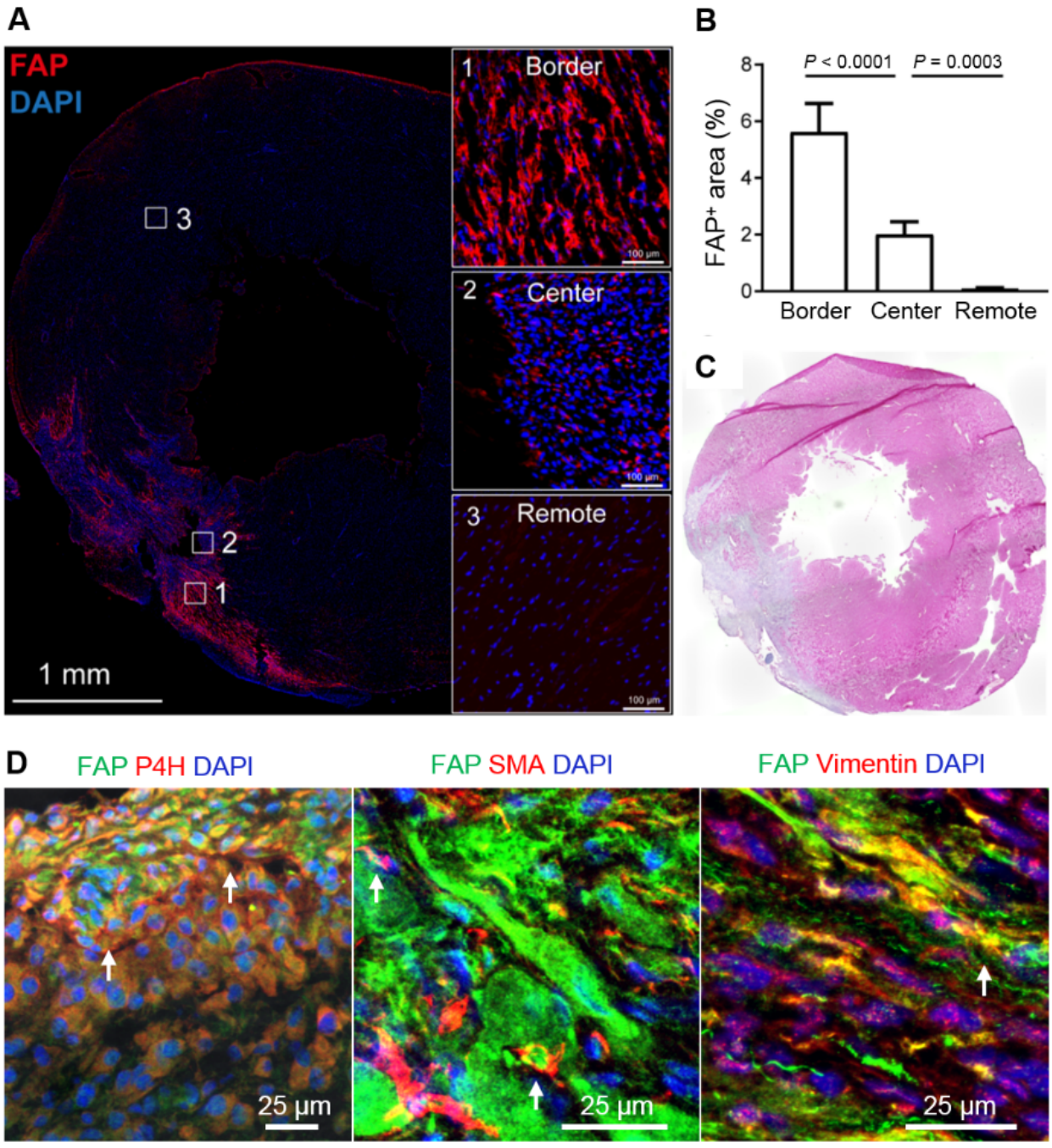

FIGURE. 7 (A) Tile scan of an entire infarcted heart section showing the location of FAP^+ fibroblasts (red). Insets 1, 2, and 3 are showing higher magnification from infarct border, infarct centre and non-infarcted remote myocardium, respectively. (B) Enumeration of FAP^+ fibroblast density in MI hearts (n=3) showed higher FAP^+ fibroblast percentage in the border zone compared

to infarct centre and remote zone. (C) H&E stained parallel section is shown. (D) Photomicrographs of FAP (green), P4H, SMA, and vimentin (red) stained infiltrated fibroblasts in the peri-infarct border zone. Abundant co-localisation of FAP, P4H and vimentin showed that accumulated fibroblasts were activated phenotypes, while a small portion of them were differentiated into SMA^{+} mature myofibrobalsts.

SUPPLEMENTAL DATA

Supplemental Table 1. The PET/CT-derived ^{68}Ga-FAPI-04 uptake (1 h p.i.) in the heart and neighbouring organs 6 days after coronary ligation (n=6).

Region	**%ID/g**	**Infarct-to-organ ratios**
Infarcted myocardium	1.0 ± 0.2	1
Non-infarcted myocardium	0.2 ± 0.1	6 ± 2
Blood	0.24 ± 0.03	4 ± 1
Liver	0.09 ± 0.04	11 ± 3
Lung	0.09 ± 0.01	9 ± 1

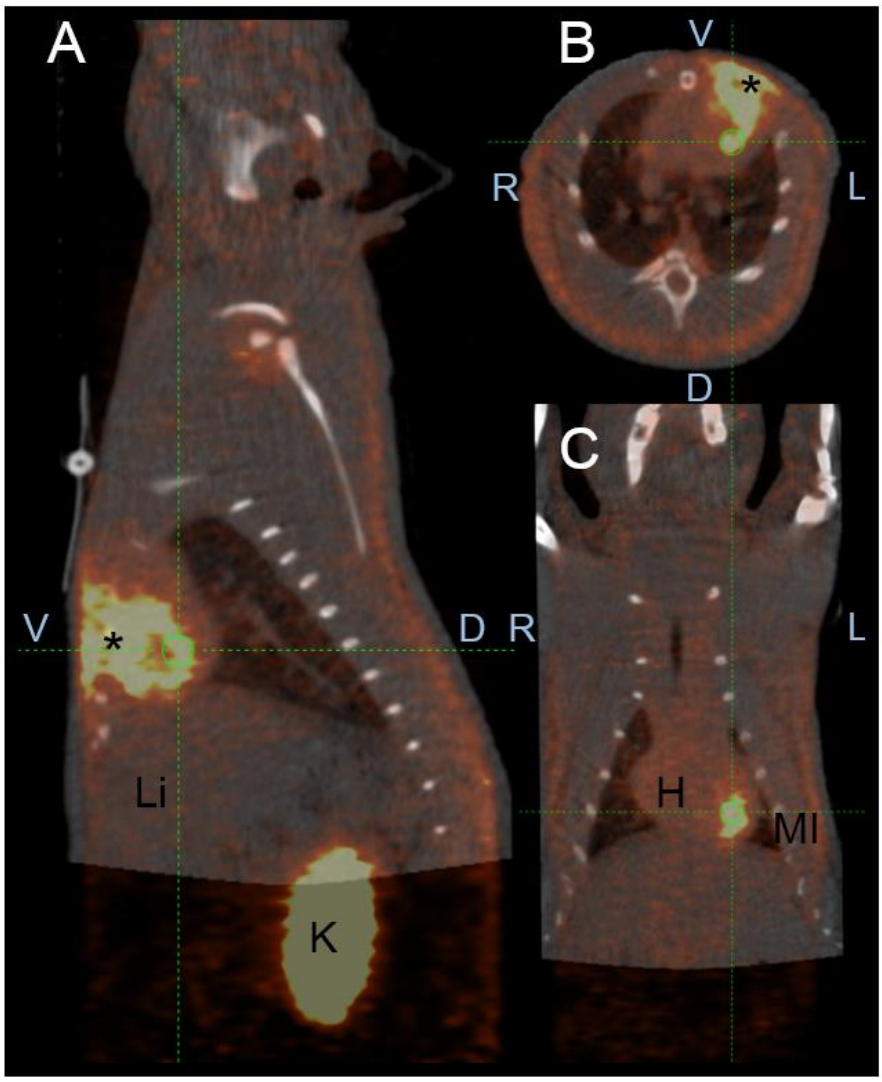

Supplemental Figure. 1 In vivo imaging of ^{68}Ga-FAPI-04 uptake. (A) Sagittal, (B) axial, and (C) coronal PET/CT images of a rat 1 h p.i. of ^{68}Ga-FAPI-04, 6 days after coronary ligation. The images demonstrate rapid clearance of ^{68}Ga-FAPI-04 from the body via renal filtration. Because of the small field of view (12.7 cm) for Siemens Inveon PET/CT, the entire length of the animal anatomy is not covered.

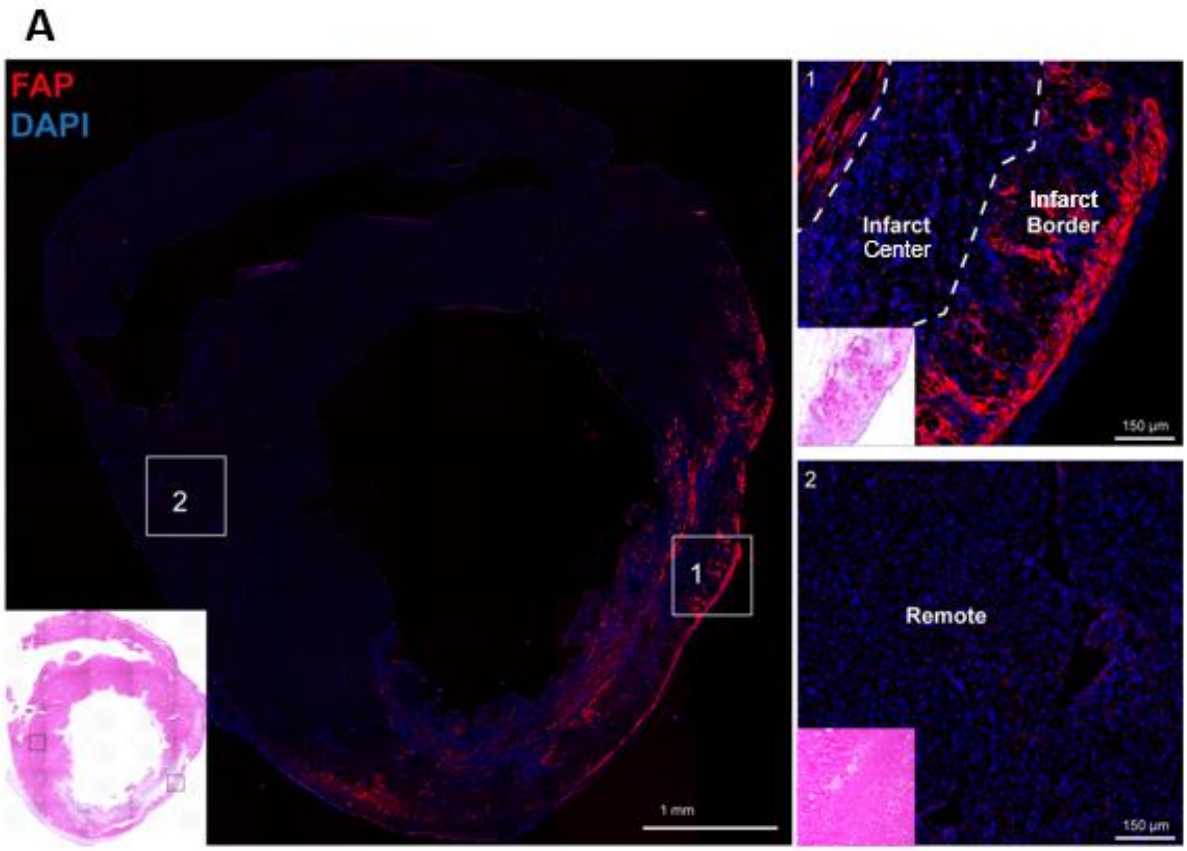
A
FAP
DAPI
2
1
1 mm
1
Infarct
Center
Infarct
Border
150 µm
2
Remote
150 µm

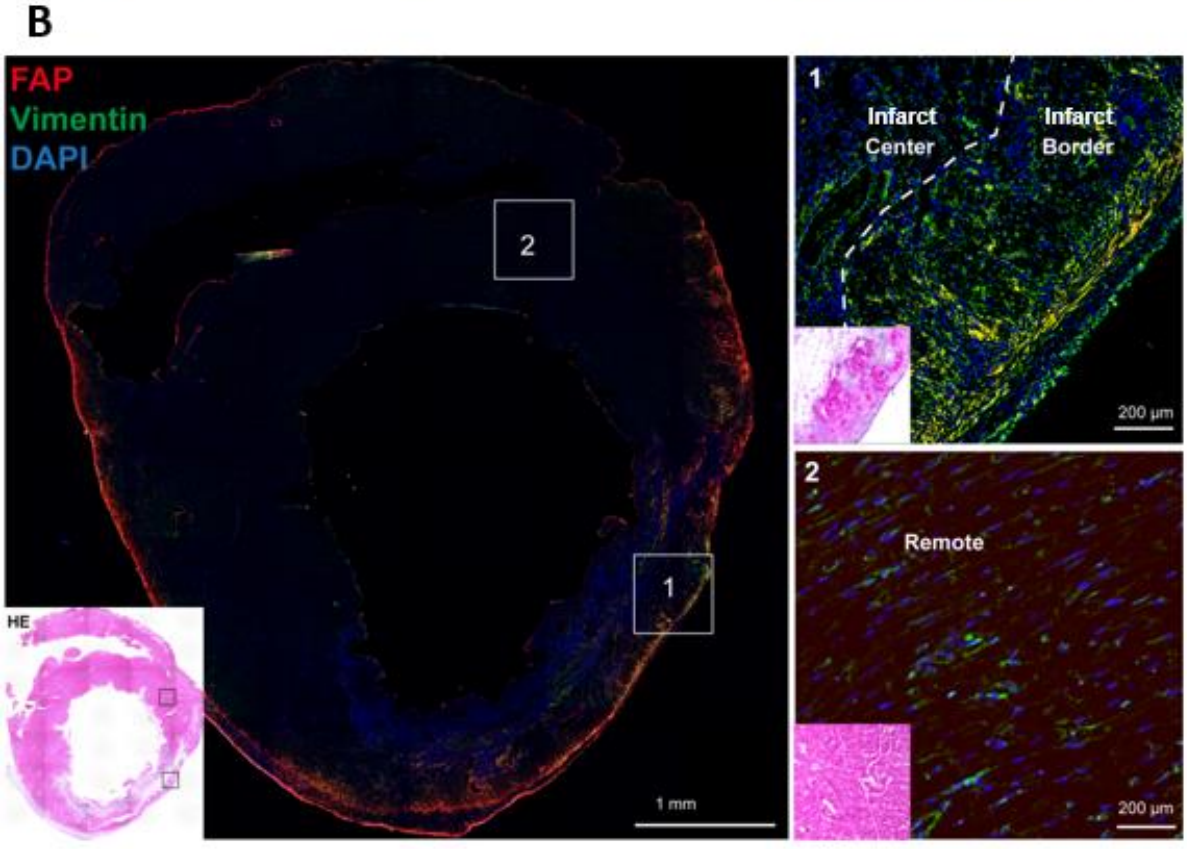
B
FAP
Vimentin
DAPI
2
1
HE
1 mm
1
Infarct
Center
Infarct
Border
200 µm
2
Remote
200 µm

Supplemental Figure. 2 Composite tile image of an entire infarcted rat heart slice and higher magnification images showing the location of FAP^+ (A) and FAP^+ $vimentin^+$ (B) fibroblasts. FAP^+ $vimentin^+$ activated fibroblasts were especially accumulated within the border zone connective tissue compared to the infract centre and remote area, while FAP^- $vimentin^+$ fibroblasts were abundant in the infarct centre or distant remote zone of the left ventricle. Overlapping domains of expression (FAP + vimentin) are shown in yellow. DAPI stained nuclei are shown in blue.

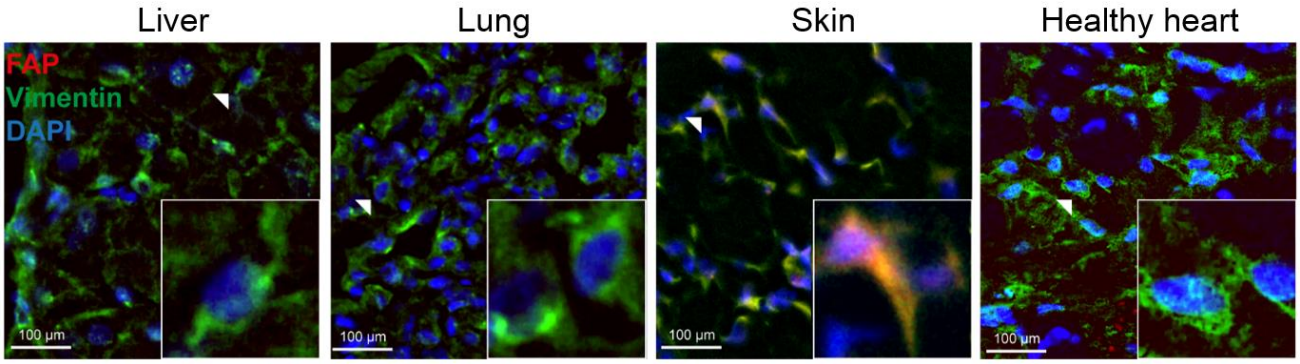

Supplemental Figure. 3 FAP expression in normal tissue-resident fibroblasts. FAP^+ cells were scarce among $vimentin^+$ fibroblasts in liver, lung, and heart of control healthy animals. FAP^+ $vimentin^+$ fibroblasts were observed in skin. Overlapping domains of expression are shown in yellow. DAPI stained nuclei are shown in blue.